Influence of Elastic Modulus Change by Springback Prediction of High Strength Steel

T. Phongsai[1,*], B. Chongthairungruang[1], V. Uthaisangsuk[2], S. Suranuntchai[1] and S. Jirathearanat[3]

[1]Department of Tool and Materials Engineering,
[2]Department of Mechanical Engineering, King Mongkut's University of Technology Thonburi,
126 PrachaUthit Rd., Bang Mod, ThungKhru, Bangkok, 10140 Thailand
[3]National Metal and Materials Technology Center,
114 Paholyotin Rd., Klong 1, KlongLuang, Pathumtani, 12120 Thailand

Abstract

The springback is caused by the release of residual stresses in a work piece after forming process. Especially, the springback effect is severe by forming high strength steel sheet. A success of the springback prediction using Finite Element (FE) forming simulation strongly depends on the applied materials model. Among various parameters of the model, elastic modulus is one of the most important factors influencing the calculation accuracy that should be considered as a function of strain. In this work, two different material models, the Hill48 and Yoshida-Uemori model were used. For both models, constant and varied elastic moduli were defined. Experimentally and numerically resulted springback of a hat shape stamped part were compared. Considering the elastic modulus change improved the accuracy of the springback prediction. The Yoshida-Uemori model showed better predictions than the Hill48 model in all cases.

Keywords: High strength steel, Springback, Elastic modulus change, FEM

1. Introduction

When a sheet metal is removed from tools after forming, the springback phenomenon occurs due to the residual stress leading to an undesired deformation. The magnitude of springback effect is nearly proportional to the Young's modulus and strain hardening behavior of material. This problem is particularly critical for high strength steels, which have been increasingly used in the automotive industries with regard to the performance improvement and light-weight design. Generally, the springback strain is an elastic strain. It is well known that the elastic strain recovery is present during loading and unloading a steel sample and it leads to a hysteresis behavior or energy loss of material. Thus, description of the elastic behavior strongly affects springback prediction of a forming simulation.

The change of elastic modulus with increasing plastic strain was firstly investigated by Lems [1]. It was found that the actual springback was larger than that calculated with a constant Young's modulus value and independent of plastic deformation. However, a constant Young's modulus was often used in many commercial FEM codes because of its simplicity. A variety of theoretical and experimental investigations of phenomenon of the Young's modulus alteration depending on plastic deformation in combination with different kinds of elasto-plastic constitutive models have been investigated. Vin et al. [2] used a simple analytical model to describe the relationship between Young's modulus and plastic deformation based on experimental results. Morestin et al. [3, 4] formulated an elasto-plastic model using a kinematic hardening model for springback analysis in sheet metal forming. The change of Young's modulus versus plastic strain was proposed. Ghosh [5] observed that slope of the elastic modulus variation was different during loading and unloading step due to the reciprocal dislocation movement. Zang et al. [6] determined the effect on sheet springback of three hardening rules, namely, an isotropic hardening, non-linear kinematic hardening and isotropic/non-linear kinematic hardening model, both constant and change of Young's modulus by a draw-bead test device. Yu [7] investigated the change of elastic modulus by simulating a U-channel forming test using LS-DYNA. The springback results from simulations and experiments were compared. Abdel-Karim [8] used the Armstrong-Frederick model and two different values for the elastic modulus during loading and unloading. The results showed that the elastic modulus could have a significant influence on springback prediction under uniaxial stress but a non- significant influence under biaxial stress. Yoshida et al. [9] noted that the elastic modulus decreased with increasing pre-strain during a cyclic tension–compression deformation. An empirical expression was proposed for the elastic modulus change, by which additional model parameters needed to be determined.

In this work, springback effects of a high strength dual phase steel according to the elastic modulus change were studied. Both experiments and FE simulations of a hat-shape stamping test were investigated. Two types of material models in combination with constant and varied elastic moduli were taken into account. One is the Hill48 model describing an isotropic yield behavior, which is often implemented in commercial FE programs. Another one is the Yoshida-Uemori kinematic hardening model, by which back stress during unloading step could be considered. The simulation results were verified by the forming experiments.

2. Materials Modeling

Elastic behavior of high strength steel during increasing plastic strain could be depicted in Fig. 1. It is clear that the average Young's moduli E_{av} decreases rapidly with increasing pre-strain ε_0^p. Then, it gradually approaches an asymptotic value. Such a pre-deformation dependency of the Young's modulus can be well expressed by the following equation:

$$E_{av} = E_0 - (E_0 - E_a)[1 - \exp(-\xi\varepsilon_0^p)] \quad (1)$$

*Corresponding Author:E-mail: dump_tme@hotmail.com

where E_0 and E_a are the Young's modulus for initial and infinitely large pre-strained materials, respectively, and ξ is a material constant.

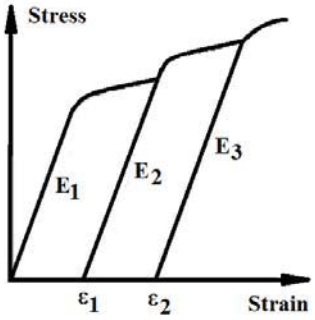

Fig. 1 Scheme of the method for measuring elastic modulus.

2.1 Planar anisotropic model with 3-R values (Hill's 1948 model)

This material model is a generalization of the well-known Von Mises yield criterion and can be simplified to a plane stress condition as given by:

$$\sigma_{xx}^2+\sigma_{yy}^2-\frac{2R}{R+1}\sigma_{xx}\sigma_{yy}+2\frac{2R+1}{R+1}\sigma_{xy}^2=\bar{\sigma}^2 \tag{2}$$

$$R=\frac{r_0+2r_{45}+r_{90}}{4} \tag{3}$$

r_0, r_{45} and r_{90} are the Lankford coefficients describing the materials anisotropy at 0°, 45°, and 90° from the rolling direction, respectively. R is the average anisotropy coefficient, while $\bar{\sigma}$ is the effective stress. This model is referred to the model MAT_37 in LS-DYNA [10] and is called Hill's 1948 planar anisotropic material model with 3-*R* values. Generally, this model is used with a constant elastic modulus. In this work, the elastic modulus change with increasing plastic strain was additionally defined.

2.2 Kinematic hardening transversely anisotropic material model (Yoshida-Uemori model)

This materials model combines Yoshida- Uemori non-linear kinematic hardening with Hill's 1948 yield criterion. The model is described by a kinematic hardening model containing a yield surface (*f*) and a boundary surface (*F*), as shown in Fig. 2. The centre of the yield surface can be displaced due to the back stress (α). *O* is the initial centre of the yield surface, α_* is the relative kinematic motion of the yield surface with respect to the bounding surface, β is the centre of the boundary surface, *Y* is the size of the yield surface, *B* is the initial size of the bounding surface, and *R* is the isotropic hardening of the bounding surface. The back stress consists of two components (β) and (α_*), which are defined by following equations:

$$\boldsymbol{\alpha}_*=\boldsymbol{\alpha}-\boldsymbol{\beta} \tag{4}$$

$$\mathring{\boldsymbol{\alpha}}_*=C\left[\frac{a}{Y}(\boldsymbol{\sigma}-\boldsymbol{\alpha})-\boldsymbol{\alpha}_*\sqrt{\frac{a}{\bar{\alpha}_*}}\right]\dot{\bar{\varepsilon}}_p \tag{5}$$

$$\dot{\bar{\varepsilon}}_p=\sqrt{\frac{2}{3}\boldsymbol{D}^p:\boldsymbol{D}^p},\ \bar{\alpha}_*=\phi(\boldsymbol{\alpha}_*),\ a=B+R-Y \tag{6}$$

$\dot{\bar{\varepsilon}}_p$ is the effective plastic strain rate, which is defined as the second invariant of D^p, and *C* is a material parameter that controls the rate of the kinematic hardening. Here, (°) stands for the objective rate. The change of size and location for the boundary surface is defined as:

$$\dot{R}=k(R_{sat}-R)\dot{\bar{\varepsilon}}_p \tag{7}$$

$$\mathring{\boldsymbol{\beta}}'=k\left(\frac{2}{3}b\boldsymbol{D}^p-\boldsymbol{\beta}'\dot{\bar{\varepsilon}}_p\right) \tag{8}$$

$$\sigma_{bound}=B+R+\beta \tag{9}$$

$\boldsymbol{\beta}'$ and $\mathring{\boldsymbol{\beta}}'$ are the deviatoric components of and its objective rate, respectively (hereafter, the prime (′) denotes the deviatoric stress component, and *b* is a material parameter. The work-hardening stagnation in unloading process shown the non-isotropic hardening surface g_σ defined in stress space, as schematically illustrated in Fig. 2(a) and (b). The isotropic hardening of the bounding surface takes place only when the center point of the bounding surface, $\boldsymbol{\beta}$, stays on the surface g_σ [see Fig. 2(b)]. In conclusion, the materials parameters *Y*, *C*, *B*, *k*, *b*, and $\boldsymbol{R}_{sat}$ are needed for the simulation. Beside these six model parameters, an additional parameter *h* is used to fit the hardening stagnation with experimental results. The kinematic hardening transversely anisotropic material model is referred to the MAT_125 model in LS-DYNA [10].

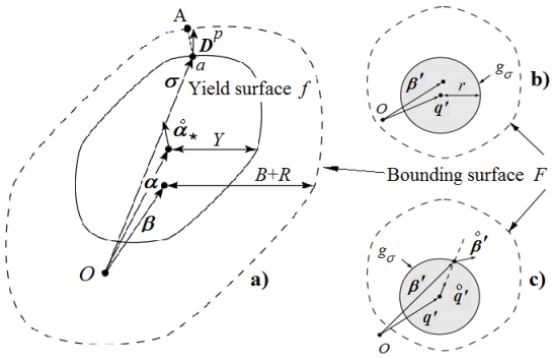

Fig. 2 Schematic description of the Yoshida-Uemori model. [10]

3. Experimental Procedure

The investigated steel was the cold-rolled high strength Dual Phase (DP) steel grade JIS SPFC780Y with the initial thickness of 1.4 mm. The chemical composition of the as-received steel sheets is presented in Table 1. The microstructure of this steel was observed under optical microscope. It consists of ferritic matrix embedded with very fine martensitic islands, as illustrated in Fig. 3.

Table 1 Chemical composition of the investigated steel (mass content in %).

C	Si	Mn	P	S	Al	Nb
0.094	0.591	2.231	0.014	0.004	0.017	0.017

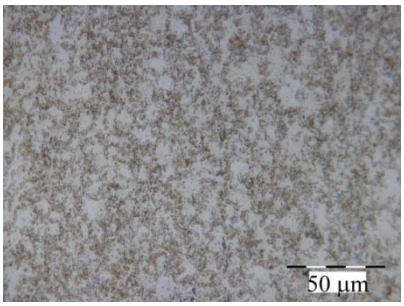

Fig. 3 Microstructure of the investigated DP steel SPFC780Y.

3.1 Uniaxial tensile test

Uniaxial tensile test were carried out to characterize anisotropic plastic behavior of the investigated steels. The specimens according to JIS:Z-2201 No.5 were used. The crosshead speed of the tests was 0.01 mm/s, which is corresponding to the strain rate of 0.0002 s^{-1}. The stress-strain curves of the steel were determined for the samples prepared in parallel, transverse and 45 degree to the rolling direction. The determined true stress-true strain curves were presented in Fig. 4. The flow curves were extrapolated with both isotropic hardening laws according to Voce and Swift, as shown in Fig. 4. The obtained mechanical properties were summarized and given in Table 2.

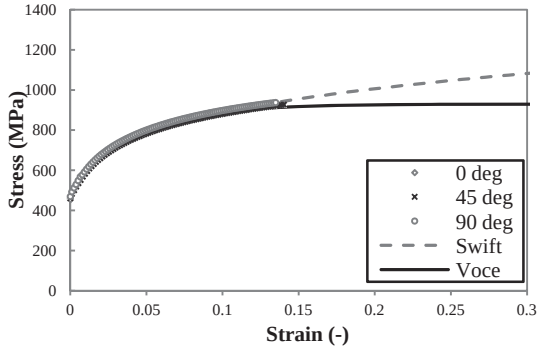

Fig. 4 Flow curves in different directions determined by uniaxial tensile tests including its extrapolations.

3.2 Determination of elastic modulus change

The loading-unloading tensile tests were carried out using the same specimens [11]. The specimen was initially elongated to a plastic strain of about 0.02 and then unloaded. Thereafter, it was further elongated with increasing a stepwise strain of 0.02. The parameters for the elastic modulus change calculated according to Eq. (1) are shown in Table 2 for the rolling direction. In Fig. 5, the true stress-true strain curves determined from uniaxial loading-unloading-reloading tensile test in the rolling direction were plotted and compared with that from the monotonic tensile test.

Table 2 Parameters describing elastic modulus change of the investigated steel in the rolling direction.

E_0 (GPa)	E_{sat} (GPa)	ξ
199.852	168.625	37.0460

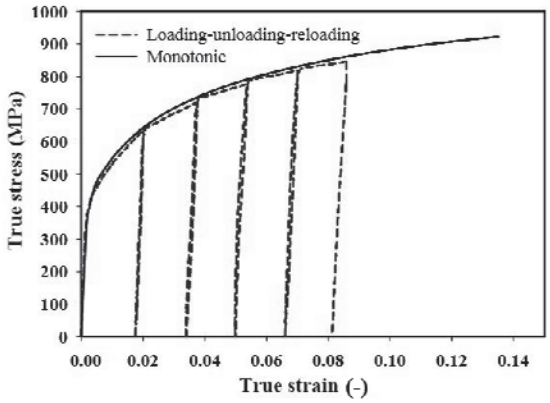

Fig. 5 Experimentally determined true stress-true strain curves from uniaxial loading-unloading-reloading tensile test in the rolling direction in comparison with monotonic tensile curve [11].

3.3 Hat-shape forming test

Hat-shape sample was used in this work to study the springback effect. Rectangular blank sheets with a length of 314 mm and a width of 50 mm were prepared from the rolling direction. The sample was formed with a drawing depth of 70 mm. The blank holder force of 35 tons was applied. Fig. 6 shows the experimental setup of the hat-shape forming test. After forming, surface scanning was performed to measure the final dimension of the formed samples, as illustrated in Fig. 7.

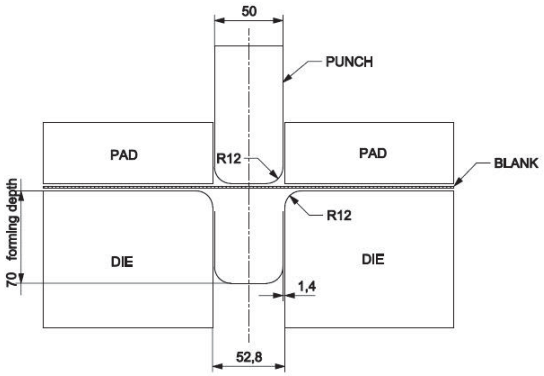

Fig. 6 Hat-shape stamping test.

Fig. 7 Formed sample of the investigated steel.

Table 3 Determined material properties of the investigated steel SPFC780Y.

Direction	E	σ_y	σ_u	Elongation (%)		r-Value	Poisson's Ratio(assumed)
	(GPa)	(MPa)	(MPa)	Uniform	Total		
00°	199.852	457.804	809.673	14.122	23.894	0.9987	0.3
45°	187.057	459.780	805.465	15.119	27.019	1.1508	0.3
90°	219.998	469.094	819.639	14.561	24.576	1.1116	0.3

4. Finite Element simulation

Numerical FE simulations of hat-shape forming test were carried out in LS-DYNA. The boundary conditions were defined according to the experiments. The blank was meshed using shell element. All of tooling parts were defined as rigid body. The friction coefficient between all contact surfaces of 0.125 was defined. The final shape of the formed samples after tool removal was calculated. In this case, the springback effect was represented by the angle between both flanges and the angle between both side-walls of the sample, as depicted in Fig. 8. After springback simulations, the springback angle and side-wall curl were determined. The angles θ_1 and θ_2 as shown were used to compare the results from experiments and simulations.

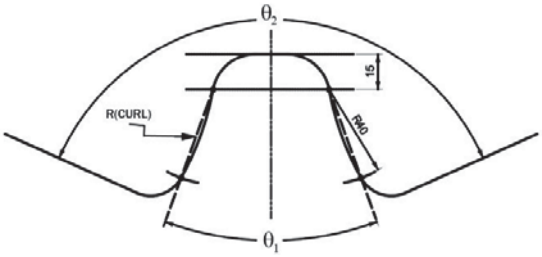

Fig. 8 Definition of resulted angles for evaluating the springback effect.

The flow curves from the rolling direction were applied in the simulations. In case of Hill48 model, the material properties used in the simulations were already shown in Table 3. The stress-strain curves were fitted by the Swift hardening law. For the Yoshida-Uemori model, the anisotropic parameter (*h*) was taken from the literature [12] and the other model parameters were determined by experiments. All parameters are summarized in Table 4. Both constant and varied elastic moduli were defined in the simulations in combination with both yield criteria.

5. Results and Discussion

Cross sections of the stamped parts after springback determined by experiment and predicted by FE simulation using different materials models are compared in Fig. 9. The simulations using varied elastic moduli provided better springback predictions for the conventional Hill48 model as well as for the kinematic Yoshida-Uemori model, as shown in Fig. 9(b) and 9(c), respectively. However, the Yoshida- Uemori model exhibited much more precise final dimension of the deformed sample than the isotropic Hill48 model, as illustrated in Fig. 9(a) and 9(b), respectively. The final shapes resulted from the simulation using Yoshida-Uemori model with varied elastic moduli fairly agreed with the experimental data.

After the tests, the springback angles θ_1 and θ_2 were measured and compared with the numerical results, as shown in Fig. 10(a) and 10(b). Additionally, curl was evaluated by measuring the radius on the side-wall of each formed sample. It was found that the Hill48 model predicted springback angles much different from the experimental results. Nevertheless, consideration of the elastic modulus change improved the results up to 1.5 degree. The Yoshida-Uemori model gave more accurate predictions than the Hill48 model, even in case of constant elastic modulus. The varied elastic moduli provided again better agreements with the experiments by the Yoshida-Uemori model. Regarding the curl prediction the results were definitely improved due to the consideration of the elastic modulus change.

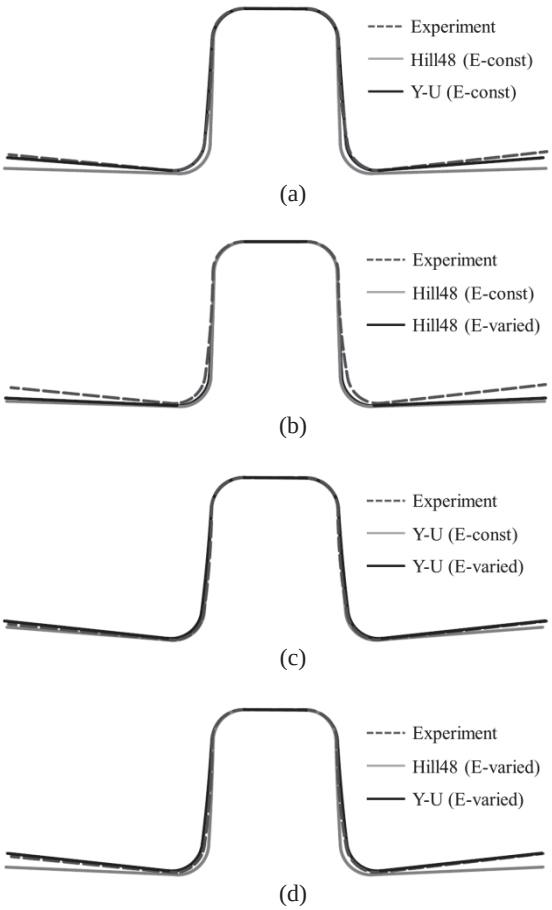

Fig. 9 Comparison of experimental and simulation results of the stamped hat-shape samples for different material models and elastic modulus change.

Table 4 Material parameters for the Yoshida-Uemori model.

Y (MPa)	C	B (MPa)	R_{sat} (MPa)	b (MPa)	m	h
452.736	477.0	607.255	316.938	39.099	15.967	0.4

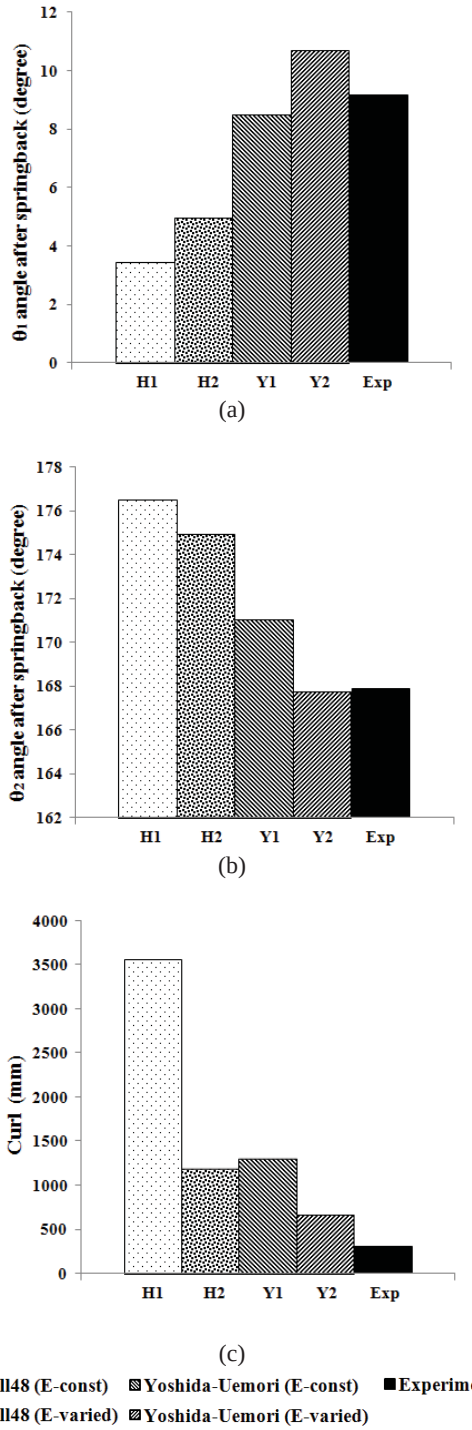

Fig. 10 Calculated springback angles (a) θ_1 (b) θ_2 and (c) curl of the stamped part with different material models and elastic modulus in comparison with experimental results.

In Fig. 11, mean stress distributed on the hat shape samples after forming calculated using different material models were illustrated. Significantly different mean stress distributions were observed for both yield criteria in combination with varied elastic moduli. This could lead to different prediction results of the springback behavior of material after forming.

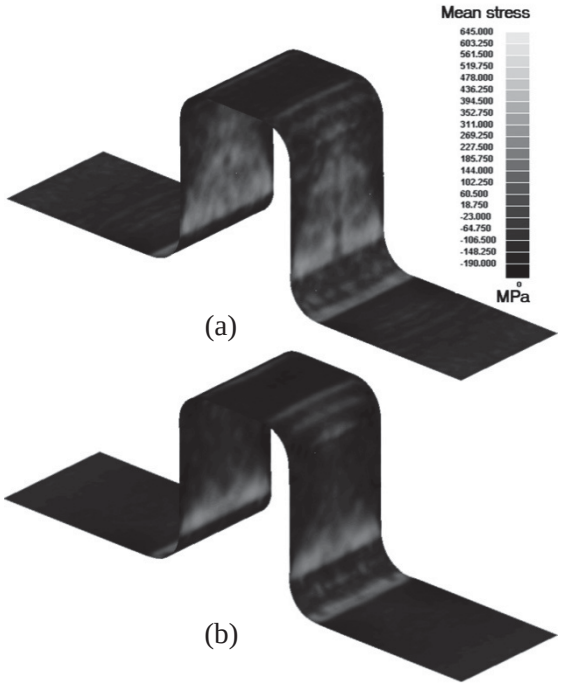

Fig. 11 Mean stress distribution on the deformed sample after forming calculated by FE simulations using (a) Hill48 and (b) Yoshida- Uemori model with varied elastic moduli.

6. Conclusion

1. The material model applying in FE simulation strongly affected prediction accuracy of the springback behavior of the high strength dual phase steel. In this study it was shown that the Yoshida-Uemori kinematic model provided springback results which much better agreed with the experiments than the conventional Hill48 model.

2. The elastic modulus change definitely influenced the prediction of springback effect, especially the curl occurrence. For the springback simulation using any material models, the elastic modulus alteration depending on the plastic deformation should be taken into accounted.

7. Acknowledgements

This work has been supported by NSTDA-University-Industry Research Collaboration (NUI-RC) and National Metal and Materials Technology Center (MTEC).

8. References

[1] Lems, W. (1963), The change of Young's modulus after deformation at low temperature and its recovery, *Ph.D. Dissertation, Delft*

[2] Vin, L.J., Streppl, A.H. and Singh, U.P. (1996). A process model for air bending, *Journal of Materials Processing Technology*, vol. 56, pp. 48–54.

[3] Morestin, F., Boivin, M. and Silva, C. (1996).Elasto-plastic formulation using a kinematic hardening model for spring-back analysis in sheetmetal forming, *Journal of Materials Processing Technology*, vol. 56, pp. 619–630.

[4] Morestin, F. and Boivin, M. (1996). On the necessity of taking into account the variation in Young's modulus with plastic strain in elastic– plastic software, *Nuclear Engineering and Design*, vol. 162, pp. 107–116.

[5] Cleveland, R. and Ghosh, A. (2002).Inelastic effects on springback in metals, *International Journal of Plasticity*, vol. 18, pp. 769-785.

[6] Zang, S.L., Liang, J. and Guo, C. (2007). A constitutive model for spring-back prediction in which the change of

Young's modulus with plastic deformation is considered, *International Journal of Machine Tools & Manufacture*, vol. 47, pp. 1791–1797
[7] Yu, H.Y. (2009). Variation of elastic modulus during plastic deformation and its influence on springback, *Materials and Design*, vol. 30, pp. 846-850.
[8] Abdel-Karim, M. (2011) Effect of elastic modulus variation during plastic deformation on uniaxial and multiaxialratchetting simulations, *European Journal of Mechanics A/Solids*, vol. 30, pp. 11-21.
[9] Yoshida, F., Uemori, T. and Fujiwara K. (2002).Elastic–plastic behavior of steel sheets underin-plane cyclic tension–compression at large strain, *International Journal Plasticity*, vol.18, pp.633–659.
[10] LS-DYNA, Keyword User's Manual Version971 Vol.2: Material Models, Livermore Software Technology Corporation, California, USA, 2007.
[11] Chongthairungruang, B., Uthaisangsuk, V., Suranuntchai, S., Jirathearanat, S. (2012). Experimental and numerical investigation of springback effect for advanced high strength dual phase steel, *Materials and Design*, vol. 39, pp. 318-328.
[12] Ma, N., Umezu, Y., Watanabe, Y. and Ogawa, T. (2008).Springback Prediction by Yoshida-Uemori Model and Compensation of Tool Surface using JSTAMP, paper presented in *proceedings of NUMISHEET 2008*, Switzerland.